ACS SENSORS

pubs.acs.org/acssensors

Article

Sensitive Detection of SARS-CoV-2 Using a SERS-Based Aptasensor

Hao Chen, Sung-Gyu Park, Namhyun Choi, Hyung-Jun Kwon, Taejoon Kang,* Mi-Kyung Lee,* and Jaebum Choo*

Cite This: https://doi.org/10.1021/acssensors.1c00596

Read Online

ACCESS | Metrics & More | Article Recommendations | Supporting Information

ABSTRACT: We developed a new surface-enhanced Raman scattering (SERS)-based aptasensor platform capable of quantifying severe acute respiratory syndrome coronavirus 2 (SARS-CoV-2) lysates with a high sensitivity. In this study, a spike protein deoxyribonucleic acid (DNA) aptamer was used as a receptor, and a self-grown Au nanopopcorn surface was used as a SERS detection substrate for the sensible detection of SARS-CoV-2. A quantitative analysis of the SARS-CoV-2 lysate was performed by monitoring the change in the SERS peak intensity caused by the new binding between the aptamer DNA released from the Au nanopopcorn surface and the spike protein in the SARS-CoV-2 virion. This technique enables detecting SARS-CoV-2 with a limit of detection (LoD) of less than 10 PFU/mL within 15 min. The results of this study demonstrate the possibility of a clinical application that can dramatically improve the detection limit and accuracy of the currently commercialized SARS-CoV-2 immunodiagnostic kit.

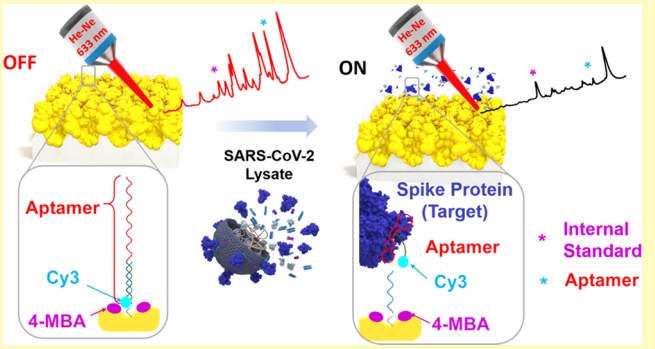

KEYWORDS: *SARS-CoV-2, COVID-19, surface-enhanced Raman scattering, aptamer, spike protein*

The severe acute respiratory syndrome coronavirus 2 (SARS-CoV-2) pandemic has caused significant social and economic problems worldwide.[1−3] Vaccines have been developed and inoculated in various countries to prevent the spread of SARS-CoV-2; however, a rapid and accurate diagnosis of the virus is also crucial. Currently, reverse transcription-polymerase chain reaction (RT-PCR), which detects ribonucleic acid (RNA) inside a virus, is used as the standard diagnostic method for SARS-CoV-2;[4−7] however, the total diagnostic time, including sample preparation, gene amplification, and detection, requires ∼3−4 h. Thus, it is necessary to shorten the diagnostic time for rapid on-site diagnosis. Various rapid kits for immunodiagnosis using antigen−antibody reactions have also been developed and commercialized to shorten the diagnosis time. However, they have not been adopted as the standard diagnostic method owing to their low limit of detection (LoD) and poor accuracy.[8−10] In particular, false negatives obtained by commercialized immunodiagnostic kits are a severe problem that can aggravate the spread of SARS-CoV-2.[11,12] Therefore, the development of a rapid and accurate immunodiagnostic technology is essential to prevent the spread of large-scale contagious infections. Innovative diagnostic technology for detecting a small amount of the virus with a new receptor having a strong binding power with SARS-CoV-2 is urgently needed to solve the issues of the currently used immunodiagnostic antigen kits.

In this study, we developed a new diagnostic assay platform that can improve the detection sensitivity of SARS-CoV-2 through surface-enhanced Raman scattering (SERS) analysis. For this purpose, we used a Au nanopopcorn substrate[13−15] and a spike protein deoxyribonucleic acid (DNA) aptamer receptor developed by Song's group.[16,17] The K_d value of the DNA aptamer for the spike protein was estimated to be 5.8 nM. The spike protein expressed on the surface of SARS-CoV-2 binds to the angiotensin-converting enzyme 2 (ACE2) receptor on the surface of human cells and penetrates the cell.[18,19] A DNA aptamer with a comparable binding affinity to the spike protein was used as a binding receptor instead of ACE2 in this study.[20,21] When diagnosing coronavirus, a nasopharyngeal smear is taken with a cotton swab and then lysed to extract proteins in the virus. We chose a SARS-CoV-2 lysate, which is close to the actual clinical sample, as the target to develop a new diagnostic method that can be used in the real clinical field. In contrast, SERS detection technology based on the electromagnetic field enhancement effect at the hot junctions of the Au nanopopcorn substrate enables the

Received: March 23, 2021
Accepted: May 11, 2021

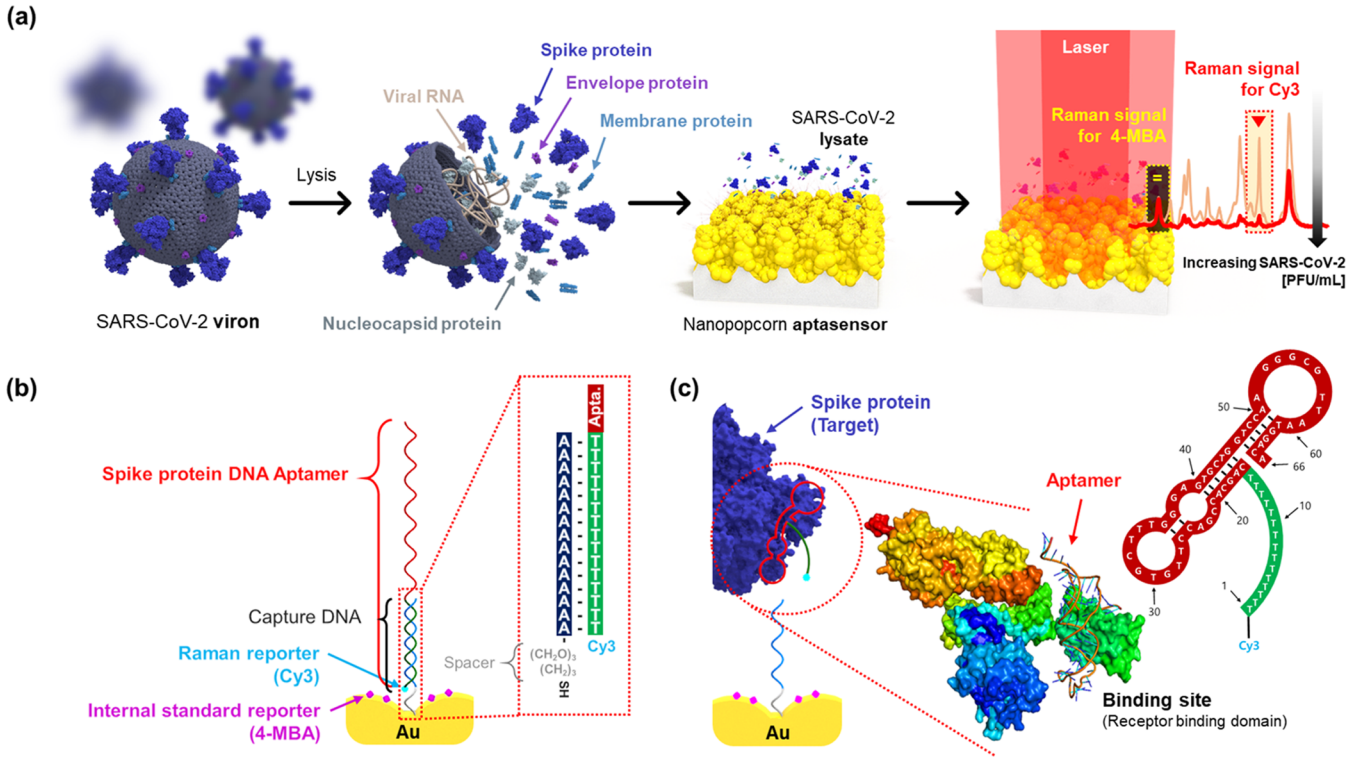

Figure 1. Schematic illustration of the quantitative evaluation of SARS-CoV-2 using the SERS-based aptasensor. (a) After SARS-CoV-2 lysates release the target spike proteins, they are recognized by the aptamer DNAs on the Au nanopopcorn surfaces. The spike protein-bound aptamers move away from the Au nanopopcorn surfaces, leading to a decreased Raman peak intensity of Cy3 reporters. (b) Cy3-tagged aptamer DNAs are hybridized with capture DNAs on the Au nanopopcorn substrate. The internal standard 4-MBAs are immobilized along with aptamer DNAs on the Au nanopopcorn substrate. (c) Recognition of the spike protein of SARS-CoV-2 induces a conformational change of aptamer DNAs, enabling the aptamer DNAs to bind with the receptor-binding domain (RBD) on the spike protein.

detection of a small number of samples compared to the fluorescence detection method commonly used in bioanalysis.[22−24] To allow the highly sensitive detection of SARS-CoV-2, the spike protein DNA aptamers, in which Raman reporter molecules are bound to its terminal, are immobilized by DNA hybridization on the Au nanopopcorn surface. When a SARS-CoV-2 lysate is added to the substrate, the DNA aptamer binds to the SARS-CoV-2 lysate. It separates from the substrate because the binding between the spike proteins released from the lysate and the aptamer is stronger than that of the DNA hybridization. At this time, the number of viruses can be quantified by monitoring the characteristic peak intensity of the Raman reporter molecules.

The new SARS-CoV-2 diagnostic method provides improved sensitivity and specificity compared with the existing lateral flow assay or enzyme-linked immunosorbent assay (ELISA). In particular, the clinical applicability of the proposed SERS aptasensor was verified using samples obtained by spiking various concentrations of the SARS-CoV-2 lysate in a transport medium solution containing nasopharyngeal swabs from negative patients. We report the quantitative analysis results obtained using the SERS aptasensor and its potential feasibility for the rapid and sensitive diagnosis of SARS-CoV-2.

EXPERIMENTAL SECTION

Materials. Ethanol (99.5%), 6-mercapto-1-hexanol (MCH), tris(2-carboxyethyl)phosphine hydrochloride (TCEP), 4-mercaptobenzoic acid (4-MBA), magnesium chloride, and saline sodium citrate (SSC) buffer (pH 7.0) were purchased from Sigma-Aldrich (St. Louis, MO). Phosphate-buffered saline (PBS) (10×, pH 7.4) was purchased from Invitrogen Corporation (Carlsbad, CA). Ultrapure water (0.055 μs/cmc) was obtained from a laboratory water system (Göttingen, Germany). Aptamer probes and capture DNA oligonucleotides were purchased from Integrated DNA Technologies, Inc. (Coralville, IA) having the sequences of 5″-Cy3/TTT TTT TTT TTT TTT CAG CAC CGA CCT TGT GCT TTG GGA GTG CTG GTC CAA GGG CGT TAAT GGA CA-3″ and 5′-AAA AAA AAA AAA AAA-$(CH_2O)_3(CH_2)_3$-SH-3′, respectively. Influenza A virus lysates were purchased from Microbix (Mississauga, Canada). Chung-Ang University Hospital provided negative SARS-CoV-2 clinical specimen samples. The research protocol for clinical samples was approved by the Institutional Review Board (IRB) of the Chung-Ang University Hospital. All chemicals used in this study were of analytical reagent grade and were used without further purification.

Instrumentation. The SERS spectra and Raman images were acquired using an in Via Renishaw Raman microscope system (Renishaw, New Mills, U.K.). A He−Ne laser operating at 632.8 nm was used as the excitation source. The Rayleigh line was removed from the Raman scattering using a holographic notch filter located along the collection path. Raman spectral data were collected using a charge-coupled device camera. The SERS mapping images were obtained by laser point mapping using a 20× (NA 0.4) objective lens with a diffraction limit of 0.9 μm. The baseline correction of Raman spectra was performed using WiRE V 4.0 software (Renishaw, New Mills, U.K.). The spectral analysis was performed using Origin Pro V8 software (OriginLab Corporation, Northants). A Cary 100 spectrometer (Varian, UT) was used to obtain the UV−visible absorption spectra. The transmission electron microscopy (TEM) images were obtained using a JEOL JEM 2100F instrument at an accelerating voltage of 200 kV. ELISA data were obtained using a microplate reader (Power Wave ×340, Bio-Tek, VT) equipped with a 96-well plate.

https://doi.org/10.1021/acssensors.1c00596
ACS Sens. XXXX, XXX, XXX−XXX

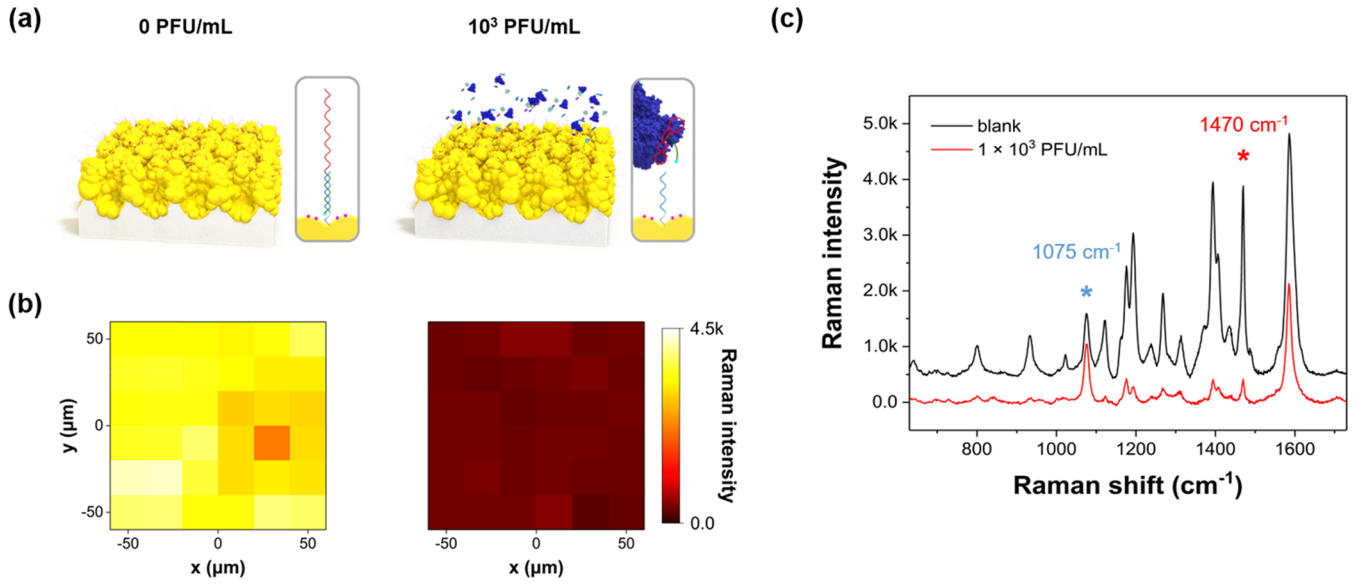

Figure 2. The on−off mechanism for the quantitative evaluation of SARS-CoV-2. (a) Schematic illustration of the SERS-based aptasensor for the on−off evaluation of the SAR-CoV-2 lysate. (b) Raman images measured with the Cy3 Raman intensity at 1470 cm^{-1} for different conditions on Au nanopopcorn substrates: aptasensor treated without target (left image) and aptasensor treated with the 10^3 PFU/mL sample (right image). The scale bar on the right presents the color coding to depict the Raman peak intensity. (c) Average Raman spectra obtained from 36 pixels of the corresponding Raman images of (b).

Fabrication of the Au Nanopopcorn Substrate. The fabrication process of the Au nanopopcorn surface has been reported elsewhere.[13,14] This plasmonic substrate was cleaned with ethanol and deionized water. To activate the thiol groups at the ends of DNA sequences, DNAs were treated with TCEP at a pH of 4 for 1 h. PBS buffer solution was added to adjust the pH value to 7. Subsequently, the substrate was incubated for 2 h in the DNA capture solution and immersed in 2 mM MCH containing a 0.1 mM 4-MBA solution at 25 °C for 2 h. It was washed with a buffer a couple of times. After the immobilization of the DNAs on the surface, they were hybridized with aptamer DNAs in 2× SSC buffer at room temperature for 2 h. Then, they were rinsed with a buffer to eliminate nonhybridized DNA aptamers and dried with nitrogen gas. Prior to the hybridization with capture DNAs, the aptamer DNAs were heated to 90 °C for 10 min to unfold their strain and then cooled to room temperature.

Preparation of SARS-CoV-2 Viral Lysates. The National Culture Collection for Pathogens (NCCP), operated by the Korea National Institute of Health, provided SARS-CoV-2 virus lysates (BetaCoV/Korea/KCDC03/2020). SARS-CoV-2 was propagated in Vero cells (ATCC No. CCL-81) in Dulbecco's modified Eagle's medium (DMEM) with 1% antibiotic−antimycotic and tosyl phenylalanyl chloromethyl ketone (TPCK) trypsin (final concentrations of 0.5 μg/mL) at 37 °C and under 5% CO_2 for 72 h. The propagated viruses were stored at −80 °C for future use. Infectious virus titers were determined by a 50% tissue culture infective dose ($TCID_{50}$) in confluent cells in 96-well microplates. All experiments using SARS-CoV-2 were performed at the Korea Centers for Disease Control and Prevention (KCDC)-approved Biosafety Level 3 (BL-3) facility of the Korea Research Institute of Bioscience and Biotechnology (KRIBB) in accordance with institutional biosafety requirements. For the preparation of viral lysates, 90 μL of virus samples was treated with 10 μL of tris(2-carboxyethyl)phosphine (TCEP)/ethylenediaminetetraacetic acid (EDTA) (final concentrations of 100 and 1 mM, respectively) and sequentially heated at 50 °C for 5 min and 64 °C for 5 min.

SARS-CoV-2 Assays Using the SERS-Based Aptasensor. For the SARS-CoV-2 assays, 5 μL of the lysate solution (0−1000 PFU/mL) was dropped onto the aptamer-immobilized Au nanopopcorn substrate, followed by incubation at room temperature for 15 min in a humid chamber. The substrate was then instantly rinsed with a washing buffer to remove the binding complexes between the aptamers and SARS-CoV-2 lysates. Raman images were measured using a mapping tool with a 20× objective lens. A computer-controlled stage was used to acquire 36 Raman spectra with a step size of 20 μm. All spectra were measured with an exposure time of 5 s.

Competitive Assay Between ACE2 and the Spike Protein DNA Aptamer. One hundred microliter of the spike protein solution (4 μg/mL) was distributed into the wells of a 96-well plate at 4 °C overnight. After incubation, the samples were washed three times with a washing buffer to remove the nonbinding proteins. Two hundred microliter of the bovine serum albumin (BSA) (5%) solution was dispensed into each well, and the plate was incubated for 60 min at room temperature to block the remaining space in each well. After incubation, the cells were washed three times with a washing buffer. The biotinylated spike protein DNA aptamer solution was diluted to a final concentration of 0.1 μM and then denatured at 90 °C for 10 min. One hundred microliter of the biotinylated aptamer solution was distributed into each well, and the plate was incubated for 2 h at room temperature. After incubation, the cells were washed three times with a washing buffer. One hundred microliter of streptavidin−horseradish peroxidase (SA−HRP) was added into each well and incubated at room temperature for 30 min to detect the biotinylated aptamer. After washing the plate three times, the TMB solution was added, and the solution was incubated for 10 min at 25 °C. The reaction was stopped by adding 0.5 N sulfuric acid, and the absorbance at 450 nm was measured for each well.

RESULTS AND DISCUSSION

Figure 1 presents a schematic illustration of the quantitative analysis method of SARS-CoV-2 using the SERS aptasensor. As shown in Figure 1a, the SARS-CoV-2 lysate was prepared by the lysis of SARS-CoV-2 virions in the TCEP/EDTA solution, and the assay was performed with the spike protein released from the SARS-CoV-2 lysate as a target. First, the spike protein aptamer DNA, labeled with the Cy3 Raman reporter at the end, was hybridized with the capture DNA bound on the Au nanopopcorn surface. As the DNA aptamer molecule recognizes the spike protein in the SARS-CoV-2 lysate, its conformational structure changes to attach to the protein. As a result, the Cy3 at the terminal of the aptamer

https://doi.org/10.1021/acssensors.1c00596
ACS Sens. XXXX, XXX, XXX−XXX

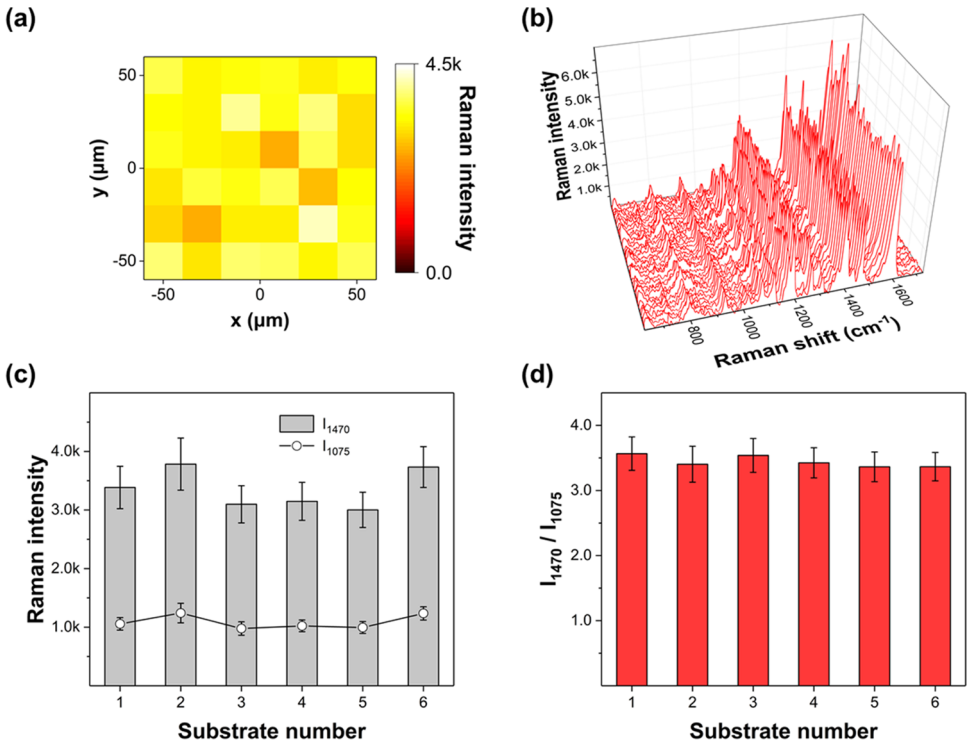

Figure 3. Improvement of detection reproducibility using the internal standard molecule (4-MBA). (a) Raman image measured with the Cy3 Raman peak intensity at 1470 cm^{-1}. (b) Raman spectra obtained from all 36 point pixels in (a). (c) Histograms for the Raman peak intensity values of the Raman reporter Cy3 (I_{1470}) and the internal standard 4-MBA (I_{1075}) collected from six different Au nanopopcorn substrates. The RSDs for six different substrates were RSD_{1470} = 9.1% and RSD_{1075} = 10%, respectively. (d) Corresponding histograms for the normalized Raman peak intensity ratios (I_{1470}/I_{1075}) for six substrates. The use of internal standards improved the RSD to 2.3%.

DNA moves away from the Au nanopopcorn surface, reducing the Raman peak intensity of Cy3. As the amount of the spike protein in the SARS-CoV-2 lysate increased, more aptamer molecules were separated from the surface of the Au nanopopcorn substrate. Consequently, the characteristic Raman peak intensity of the Cy3 molecule decreases, as shown in Figure 1a, and its monitoring enables the quantitative analysis of the spike protein in SARS-CoV-2. Figure 1b presents 15 A−T hybridization spacers to immobilize the spike protein aptamer DNAs on the Au nanopopcorn surface. Herein, 4-MBA molecules were used as internal standards to improve the reproducibility of the assay results. Figure S1a shows the average SERS spectra of 4-MBA, Cy3, and their 1:1 molar mixtures for 36 spots on the nanopopcorn substrate. As shown in this figure, these two Raman reporters appear in independent regions due to relatively little overlap with other Raman peaks. The SERS peak of Cy3 appears at 1470 cm^{-1} and that of MBA seems at 1075 cm^{-1}. The SEM image of the nanopopcorn substrate used in this study is demonstrated in Figure S1b. A molecular dynamics simulation was performed to better understand the binding site between the aptamer DNA molecule and the spike protein; the results are shown in Figure 1c. The aptamer DNA is separated from the substrate and then bound to the spike protein because the binding affinity between the aptamer DNA and the spike protein is significantly greater than the adenine (A)−thymine (T) DNA hybridization energy.

Prior to performing the SARS-CoV-2 assay using the SERS-based aptasensor, the binding capability of the aptamer to the SARS-CoV-2 spike protein was tested. Figure S2a shows a schematic illustration of the assay between the SARS-CoV-2 spike protein and the DNA aptamer. Figure S2b displays the corresponding calibration curve of the aptamer in the 0−1.0 μM range. When DNA aptamers are bound to spike proteins, the absorbance increases along with the aptamer concentration. According to this assay result, the DNA aptamer apparently has a binding affinity of comparable intensity to the ACE2 receptor with respect to the spike protein. Figure 2a shows a schematic illustration of the SERS-based aptasensor for the "on−off" test for detecting the SARS-CoV-2 lysate. Figure 2b (left) presents a Raman mapping image (6 × 6 = 36 mapping spots) of Cy3-tagged aptamer DNAs hybridized with probe DNAs on a Au nanopopcorn surface. The Raman mapping image was obtained by color decoding Raman peak intensity variation at 1470 cm^{-1} of the Raman reporter Cy3. The mapping image shows a strong SERS signal owing to the localized surface plasmon effect because the Cy3 Raman reporter molecule is significantly close to the substrate surface. With the addition of the 10^3 PFU/mL SARS-CoV-2 lysate, aptamer DNAs moved away from the substrate surface by binding to the spike protein in the SARS-CoV-2 lysate, and the corresponding Raman peak intensity decreased along with the amount of SARS-CoV-2 (Figure 2b, right). Figure 2c presents the average Raman spectra for 36 spots in each Raman mapping image in Figure 2b. The concentration of SARS-CoV-2 can be determined by monitoring the change in the Raman peak intensity at 1470 cm^{-1}.

One of the most critical issues in the quantitative analysis using SERS technology is securing the reproducibility of the substrate. To confirm the reproducibility of the Au nanopopcorn substrate used in this study, a 10^{-3} M Cy3-tagged DNA aptamer, hybridized with the capture DNA, was

https://doi.org/10.1021/acssensors.1c00596
ACS Sens. XXXX, XXX, XXX−XXX

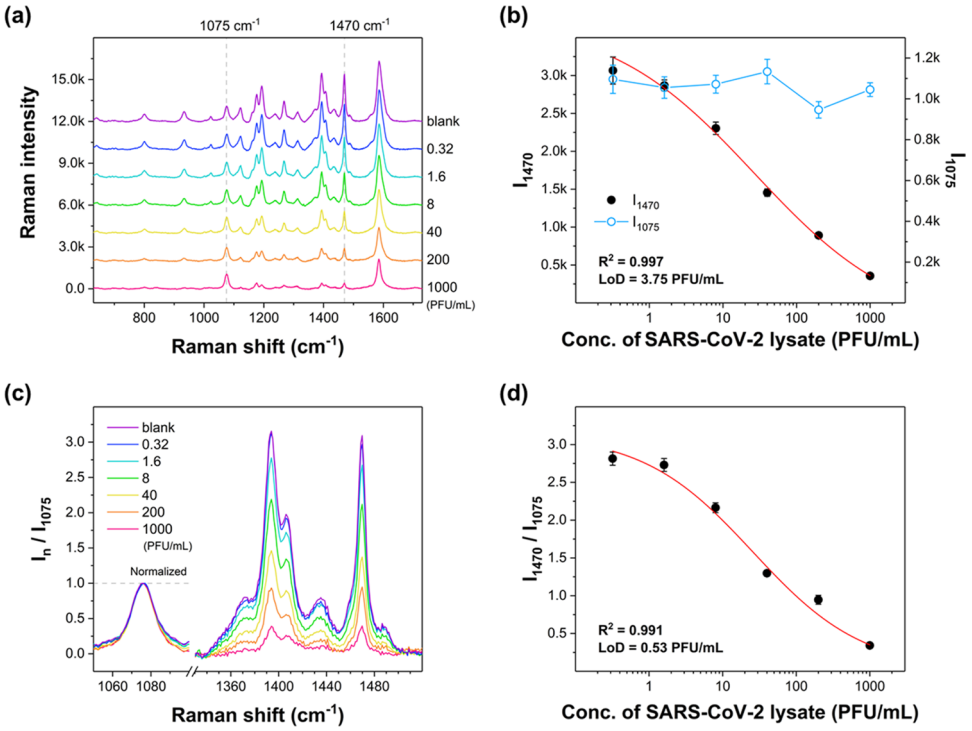

Figure 4. (a) Evaluation of Raman peak intensity variations with increasing SARS-CoV-2 concentration in PBS buffer. (a) Average Raman spectra of 36 Raman mapping points for SARS-CoV-2. The concentrations ranged from 0 to 1000 PFU/mL. (b) Variation of the average Raman peak intensity at 1470 cm^{-1} as a function of the SARS-CoV-2 lysate concentration in PBS buffer. Correlation coefficient, R^2 = 0.997. The LoD of the SARS-CoV-2 lysate was estimated to be 3.75 PFU/mL. The upper line indicates the variation of the Raman peak intensity of the internal standard (4-MBA) at 1075 cm^{-1} on the Au nanopopcorn substrates. (c) Average Raman spectra of the SARS-CoV-2 lysate for the Raman reporter Cy3 (I_{1470}) and the internal standard 4-MBA (I_{1075}) collected from six different Au nanopopcorn substrates. (d) Variation of normalized Raman peak intensity ratios of (I_{1470}/I_{1075}) as a function of the SARS-CoV-2 lysate concentration. Correlation coefficient, R^2 = 0.991. The LoD of SARS-CoV-2 lysate was estimated to be 0.53 PFU/mL.

immobilized on six different Au nanopopcorn substrates (120 μm × 120 μm), and then the Raman mapping image (6 × 6 = 36 mapping points) for each substrate was measured. Figure 3a shows the corresponding Raman mapping image on the first substrate (#1). Figure S3a shows the Raman images obtained from the Cy3 Raman peak intensity at 1470 cm^{-1} on other Au nanopopcorn substrates from #2 to #6. Figure 3b displays the corresponding average Raman spectra for the 36 mapping spots of substrate #1. Figure 3c shows the distribution and relative standard deviation (RSD) of the average values of 36 spots on six different Au nanopopcorn substrates. The RSD value is 9.1%, which indicates acceptable spot-to-spot variations; however, the confidence level is expected to increase if the internal standard is considered for each measurement. Therefore, 4-MBA was also immobilized with the aptamer DNAs on the substrate and used as an internal standard. The graph at the bottom of Figure 3c presents the substrate-to-substrate change of the Raman peak intensity of 4-MBA at 1075 cm^{-1} for six different substrates. The error bars represent the relative standard deviations for the spot-to-spot variation on the same substrate. The RSD of 4-MBA was estimated to be 10.0%. To improve the detection reproducibility, the Raman peak intensity value of the Raman reporter Cy3 (I_{1470}) was normalized to that of the internal standard 4-MBA (I_{1075}). Figure 3d demonstrates the corresponding histograms for the normalized Raman peak intensity ratios (I_{1470}/I_{1075}) for the six Au substrates, which improved the RSD to 2.3%.

Figure 4a presents the change in the average Raman spectrum with increasing virus concentration in the 0−1000 PFU/mL range of SARS-CoV-2 in PBS buffer. The Raman spectrum for each concentration was obtained by averaging 36 pixel points in the Raman mapping image in Figure S4a. The Raman peak intensity at 1470 cm^{-1} of the Cy3 Raman reporter gradually decreased with increasing virus concentration. In addition, the Raman peak intensity at 1075 cm^{-1} of 4-MBA was used as the internal standard to correct errors that may have occurred in the substrate environment or minute volume changes during the measurement. Figure 4b shows the Raman peak intensity variations at 1470 cm^{-1} (Cy3, red line) and at 1075 cm^{-1} (4-MBA, sky blue line). Raman mapping images measured at 1075 cm^{-1}, for various SARS-CoV-2 lysate concentrations ranging from 0 to 1000 PFU/mL, are shown in Figure S3b. As shown in this figure, the image remains evenly distributed over the surface, but the average Raman peak intensities show slight fluctuations, as shown in Figure 4b. Figure 4c shows the change in the relative Raman peak intensity (I_{1470}/I_{1075}) according to the SARS-CoV-2 concentration. Here, the Raman peak intensity at 1470 cm^{-1} of Cy3 was corrected by the normalized Raman peak intensity at 1075 cm^{-1} of 4-MBA. The normalized Raman spectrum for each concentration was obtained by averaging 36 pixel points in the Raman mapping image in Figure S4b. Figure 4d shows a normalized calibration curve representing the relative Raman peak intensity variation for the change in the SARS-CoV-2 concentration. When calibrated using the internal standard, the correlation coefficient value was similar to that of the nonuse;

https://doi.org/10.1021/acssensors.1c00596
ACS Sens. XXXX, XXX, XXX−XXX

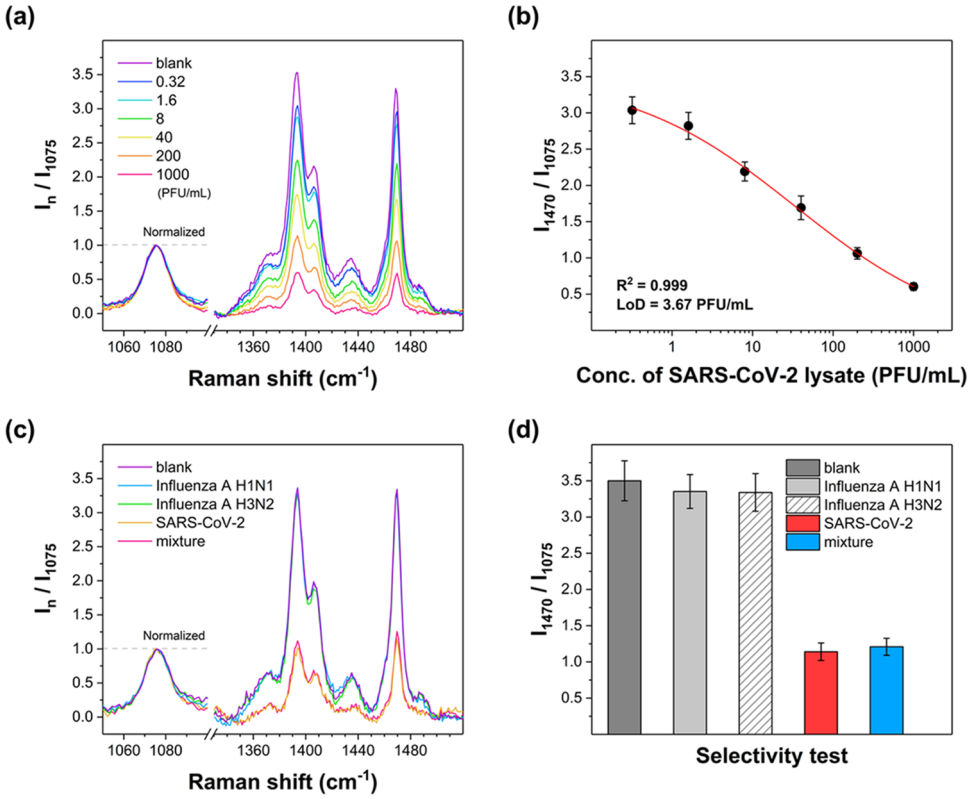

Figure 5. Evaluation of Raman peak intensity variations with increasing SARS-CoV-2 concentration in real clinical negative respiratory specimens. (a) Average Raman spectra of the SARS-CoV-2 lysate for the Raman reporter Cy3 (I_{1470}) and the internal standard 4-MBA (I_{1075}) collected from six different Au nanopopcorn substrates. (b) Variation of normalized Raman peak intensity ratios of (I_{1470}/I_{1075}) as a function of the SARS-CoV-2 lysate concentration. The SARS-CoV-2 lysate was spiked into negative respiratory specimens in the 0−1000 PFU/mL concentration range. Correlation coefficient, R^2 = 0.999. The LoD of the SARS-CoV-2 lysate was estimated to be 3.67 PFU/mL. (c) Average Raman spectra for a blank, influenza A/H1N1 (4500 PFU/mL), influenza A/H3N2 (15 000 PFU/mL), SARS-Cov-2 (200 PFU/mL), and their mixtures for the selectivity test. (d) Corresponding histograms for the normalized Raman peak intensity ratios (I_{1470}/I_{1075}) collected from (c).

however, the RSD value decreased by ∼8.0%, indicating better reproducibility. Furthermore, the LoD value became significantly lower, dropping from 3.75 to 0.53 PFU/mL, indicating that it is possible to detect very low concentrations of SARS-CoV-2. Herein, the LoD was determined from the four-parameter equation in Figure S5.

To evaluate the clinical effectiveness of this SERS-based aptasensor, assays were also performed on a solution obtained by spiking various concentrations of the SARS-CoV-2 lysate into a transport medium solution, including nasopharyngeal swabs from negative patients (clinical sample). The Cy3 SERS peak intensity representing the change in the concentration of the aptamer DNA was corrected by the normalized Raman peak intensity of the internal standard 4-MBA, as shown for the PBS buffer solution in Figure 4c. Figure 5a presents the average Raman spectra for various concentrations of the SARS-CoV-2 lysate spiked into a clinical sample. As with the PBS solution, the normalized Raman spectrum for each concentration was obtained by averaging 36 pixel points shown in the Raman mapping image in Figure S6. Figure 5b demonstrates the corresponding calibration curve for the relative SERS peak intensity that was corrected using the internal standard. The quantitative analysis results (LoD and RSD) of SARS-CoV-2 in Figure 5b are slightly higher (3.67 PFU/mL) than those measured from the PBS buffer solution. Therefore, the SARS-CoV-2 analysis using a SERS-based aptasensor is expected to function sufficiently in real clinical samples, although it was difficult to test real clinical samples of patients infected with SARS-CoV-2 owing to safety issues. Finally, assays were performed for SARS-CoV-2 (200 PFU/mL), influenza A/H1N1 (4500 PFU/mL), influenza A/H3N2 (15 000 PFU/mL), and their cocktail mixtures to evaluate the selectivity performance of the SERS aptasensor; Figure 5c presents their normalized Raman spectra, and Figure 5d displays a histogram of the Raman peak intensity changes for four different samples. The Raman spectra for each sample were obtained by averaging 36 pixel points in the Raman mapping image in Figure S7. As shown in the figures, only SARS-CoV-2 and the cocktail mixture containing it presented a significant decrease in the Raman peak intensity compared to the blank sample. The assay results demonstrated that the SERS-based aptasensor showed high selectivity for SARS-CoV-2.

CONCLUSIONS

To cope with the rapid spread of SARS-CoV-2, a conceptually new diagnostic assay platform that can improve the sensitivity of the currently commercialized LFA kit is required. In this study, a SERS-based immunodiagnostic sensor using spike protein aptamers was developed for the sensitive detection of SARS-CoV-2. The highly sensitive detection of SARS-CoV-2 was achieved by monitoring the change in the SERS peak intensity using a combination of the Au nanopopcorn substrates, which are capable of implementing a high-density hot spot, and the spike protein aptamer DNAs. In addition, the detection reproducibility of SARS-CoV-2 was improved by

https://doi.org/10.1021/acssensors.1c00596
ACS Sens. XXXX, XXX, XXX−XXX

correcting the SERS peak intensity for the Cy3 Raman tag at the terminal of the aptamer DNA using the 4-MBA molecule as an internal standard. As a result, it was possible to detect SARS-CoV-2 with an LoD of lower than 10 PFU/mL in 15 min, which presents a sensitivity of 2 orders of magnitude better than that of a commercial immunoassay rapid kit (300−500 PFU/mL). The sample obtained by spiking SARS-CoV-2 into a transport medium solution containing nasopharyngeal swabs from negative patients also presented a similar LoD value and sufficient quantitative properties, thus demonstrating the potential for a rapid and accurate diagnosis of SARS-CoV-2. To apply this SERS-based aptasensor to actual clinical practice, the research to implement a Au nanopopcorn substrate-based aptasensor with a portable Raman spectrophotometer is underway.

■ ASSOCIATED CONTENT

Supporting Information

The Supporting Information is available free of charge at https://pubs.acs.org/doi/10.1021/acssensors.1c00596.

Additional figures for average SERS spectra of two Raman reporters and the SEM image of the nanopopcorn substrate (Figure S1); schematic illustration of the assay between the SARS-CoV-2 spike protein and the DNA aptamer (Figure S2); Raman mapping images for five different Au nanopopcorn substrates and internal standards (Figure S3); Raman mapping images of various SARS-CoV-2 lysate concentrations in PBS buffer (Figure S4); four-parameter equation to determine the LoD of the SARS-CoV-2 lysate (Figure S5); normalized Raman mapping images of various SARS-CoV-2 lysate concentrations in clinically negative respiratory specimens (Figure S6); and normalized Raman mapping images of different biomarkers for the selectivity test in clinically negative respiratory specimens (Figure S7) (PDF)

■ AUTHOR INFORMATION

Corresponding Authors

Taejoon Kang − *Bionanotechnology Research Center, Korea Research Institute of Bioscience and Biotechnology (KRIBB), Daejeon 34141, South Korea;* orcid.org/0000-0002-5387-6458; Email: kangtaejoon@kribb.re.kr

Mi-Kyung Lee − *Department of Laboratory Medicine, Chung-Ang University College of Medicine, Seoul 06973, South Korea*; Email: cpworld@cau.ac.kr

Jaebum Choo − *Department of Chemistry, Chung-Ang University, Seoul 06974, South Korea;* orcid.org/0000-0003-3864-6459; Email: jbchoo@cau.ac.kr

Authors

Hao Chen − *Department of Chemistry, Chung-Ang University, Seoul 06974, South Korea*

Sung-Gyu Park − *Advanced Nano-Surface Department, Korea Institute of Materials Science (KIMS), Changwon 51508, South Korea;* orcid.org/0000-0002-0580-3211

Namhyun Choi − *Department of Chemistry, Chung-Ang University, Seoul 06974, South Korea*

Hyung-Jun Kwon − *Functional Biomaterial Research Center, Korea Research Institute of Bioscience and Biotechnology (KRIBB), Jeongup 56212, South Korea*

Complete contact information is available at: https://pubs.acs.org/10.1021/acssensors.1c00596

Author Contributions

H.C. and S.-G.P. contributed equally; T.K., M.-K.L., and J.C. designed and supervised the research; H.C. and N.C. conducted the SERS aptasensor-based assays for SARS-CoV-2 lysates; S.-G.P. fabricated Au nanopopcorn substrates; H.-J.K. prepared SARS-CoV-2 lysates; and T.K., M.-K.L., and J.C. contributed to writing the manuscript. All the authors discussed and approved the manuscript.

Notes

The authors declare no competing financial interest.

■ ACKNOWLEDGMENTS

This work was supported by the National Research Foundation of Korea (Grant numbers 2019R1A2C3004375, 2020R1A5A1018052, 2019R1C1C1006867, and 2018M3A9E2022821), the Government-Wide R&D Fund for the Research of Infectious Diseases in Korea (Grant number HG18C0062), the Center for BioNano Health-Guard funded by the Ministry of Science and ICT (MSIT) of Korea as Global Frontier Project (H-GUARD_2013M3A6B2078950), Nanomedical Devices Development Project of NNFC, and the KRIBB Research Initiative Program (1711134081).

■ REFERENCES

(1) Zhu, N.; Zhang, D.; Wang, W.; Li, X.; Yang, B.; Song, J.; Zhao, X.; Huang, B.; Shi, W.; Lu, R.; Niu, P.; Zhan, F.; Ma, X.; Wang, D.; Xu, W.; Wu, G.; Gao, G. F.; Tan, W. A Novel Coronavirus from Patients with Pneumonia in China, 2019. *N. Engl. J. Med.* **2020**, *382*, 727−733.

(2) He, X.; Lau, E. H. Y.; Wu, P.; Deng, X.; Wang, J.; Hao, X.; Lau, Y. C.; Wong, J. Y.; Guan, Y.; Tan, X.; Mo, X.; Chen, Y.; Liao, B.; Chen, W.; Hu, F.; Zhang, Q.; Zhong, M.; Wu, Y.; Zhao, L.; Zhang, F.; Cowling, B. J.; Li, F.; Leung, G. M. Temporal Dynamics in Viral Shedding and Transmissibility of COVID-19. *Nat. Med.* **2020**, *26*, 672−675.

(3) Ferretti, L.; Wymant, C.; Kendall, M.; Zhao, L.; Nurtay, A.; Abeler-Dörner, L.; Parker, M.; Bonsall, D.; Fraser, C. Quantifying SARS-CoV-2 Transmission Suggests Epidemic Control with Digital Contact Tracing. *Science* **2020**, *368*, No. eabb6936.

(4) Shen, M.; Zhou, Y.; Ye, J.; Al-Maskri, A. A. A.; Kang, Y.; Zeng, S.; Cai, S. Recent Advances and Perspectives of Nucleic Acid Detection for Coronavirus. *J. Pharm. Anal.* **2020**, *10*, 97−101.

(5) Corman, V. M.; Landt, O.; Kaiser, M.; Molenkamp, R.; Meijer, A.; Chu, D. K.; Bleicker, T.; Brünink, S.; Schneider, J.; Schmidt, M. L.; Mulders, D. G.; Haagmans, B. L.; van der Veer, B.; van den Brink, S.; Wijsman, L.; Goderski, G.; Romette, J. L.; Ellis, J.; Zambon, M.; Peiris, M.; Goossens, H.; Reusken, C.; Koopmans, M. P.; Drosten, C. Detection of 2019 Novel Coronavirus (2019-NCoV) by Real-Time RT-PCR. *Eurosurveillance* **2020**, *25*, No. 2000045.

(6) Broughton, J. P.; Deng, X.; Yu, G.; Fasching, C. L.; Servellita, V.; Singh, J.; Miao, X.; Streithorst, J. A.; Granados, A.; Sotomayor-Gonzalez, A.; Zorn, K.; Gopez, A.; Hsu, E.; Gu, W.; Miller, S.; Pan, C.-Y.; Guevara, H.; Wadford, D. A.; Chen, J. S.; Chiu, C. Y. CRISPR−Cas12-Based Detection of SARS-CoV-2. *Nat. Biotechnol.* **2020**, *38*, 870−874.

(7) Bwire, G. M.; Majigo, M. V.; Njiro, B. J.; Mawazo, A. Detection Profile of SARS-CoV-2 Using RT-PCR in Different Types of Clinical Specimens: A Systematic Review and Meta-Analysis. *J. Med. Virol.* **2021**, *93*, 719−725.

(8) Ghodake, G. S.; Shinde, S. K.; Kadam, A. A.; Saratale, R. G.; Saratale, G. D.; Syed, A.; Elgorban, A. M.; Marraiki, N.; Kim, D.-Y. Biological Characteristics and Biomarkers of Novel SARS-CoV-2 Facilitated Rapid Development and Implementation of Diagnostic

Tools and Surveillance Measures. *Biosens. Bioelectron.* **2021**, *177*, No. 112969.
(9) Li, Z.; Yi, Y.; Luo, X.; Xiong, N.; Liu, Y.; Li, S.; Sun, R.; Wang, Y.; Hu, B.; Chen, W.; Zhang, Y.; Wang, J.; Huang, B.; Lin, Y.; Yang, J.; Cai, W.; Wang, X.; Cheng, J.; Chen, Z.; Sun, K.; Pan, W.; Zhan, Z.; Chen, L.; Ye, F. Development and Clinical Application of a Rapid IgM-IgG Combined Antibody Test for SARS-CoV-2 Infection Diagnosis. *J. Med. Virol.* **2020**, *92*, 1518−1524.
(10) Xu, L.; Li, D.; Ramadan, S.; Li, Y.; Klein, N. Facile Biosensors for Rapid Detection of COVID-19. *Biosens. Bioelectron.* **2020**, *170*, No. 112673.
(11) Vandenberg, O.; Martiny, D.; Rochas, O.; van Belkum, A.; Kozlakidis, Z. Considerations for Diagnostic COVID-19 Tests. *Nat. Rev. Microbiol.* **2021**, *19*, 171−183.
(12) Mak, G. C. K.; Cheng, P. K. C.; Lau, S. S. Y.; Wong, K. K. Y.; Lau, C. S.; Lam, E. T. K.; Chan, R. C. W.; Tsang, D. N. C. Evaluation of Rapid Antigen Test for Detection of SARS-CoV-2 Virus. *J. Clin. Virol.* **2020**, *129*, No. 104500.
(13) Chen, H.; Park, S.-G.; Choi, N.; Moon, J.-I.; Dang, H.; Das, A.; Lee, S.; Kim, D.-G.; Chen, L.; Choo, J. SERS imaging-based aptasensor for ultrasensitive and reproducible detection of influenza virus A. *Biosens. Bioelectron.* **2020**, *167*, No. 112496.
(14) Park, S.-G.; Xiao, X.; Min, J.; Mun, C.; Jung, H. S.; Giannini, V.; Weissleder, R.; Maier, S. A.; Im, H.; Kim, D.-H. Self-Assembly of Nanoparticle-Spiked Pillar Arrays for Plasmonic Biosensing. *Adv. Funct. Mater.* **2019**, *29*, No. 1904257.
(15) Lu, W.; Singh, A. K.; Khan, S. A.; Senapati, D.; Yu, H.; Ray, P. C. Gold Nano-Popcorn-Based Targeted Diagnosis, Nanotherapy Treatment, and In Situ Monitoring of Photothermal Therapy Response of Prostate Cancer Cells Using Surface-Enhanced Raman Spectroscopy. *J. Am. Chem. Soc.* **2010**, *132*, 18103−18144.
(16) Song, Y.; Song, J.; Wei, X.; Huang, M.; Sun, M.; Zhu, L.; Lin, B.; Shen, H.; Zhu, Z.; Yang, C. Discovery of Aptamers Targeting the Receptor-Binding Domain of the SARS-CoV-2 Spike Glycoprotein. *Anal. Chem.* **2020**, *92*, 9895−9900.
(17) Liu, R.; He, L.; Hu, Y.; Luo, Z.; Zhang, J. A Serological Aptamer-Assisted Proximity Ligation Assay for COVID-19 Diagnosis and Seeking Neutralizing Aptamers. *Chem. Sci.* **2020**, *11*, 12157−12164.
(18) Yang, J.; Petitjean, S. J. L.; Koehler, M.; Zhang, Q.; Dumitru, A. C.; Chen, W.; Derclaye, S.; Vincent, S. P.; Soumillion, P.; Alsteens, D. Molecular Interaction and Inhibition of SARS-CoV-2 Binding to the ACE2 Receptor. *Nat. Commun.* **2020**, *11*, No. 4541.
(19) Chan, K. K.; Dorosky, D.; Sharma, P.; Abbasi, S. A.; Dye, J. M.; Kranz, D. M.; Herbert, A. S.; Proko, E. Engineering Human ACE2 to Optimize Binding to the Spike Protein of SARS Coronavirus 2. *Science* **2020**, *369*, 1261−1265.
(20) Zhang, L.; Fang, X.; Liu, X.; Ou, H.; Zhang, H.; Wang, J.; Li, Q.; Cheng, H.; Zhang, W.; Luo, Z. Discovery of sandwich type COVID-19 nucleocapsid protein DNA aptamers. *Chem. Commun.* **2020**, *56*, 10235−10238.
(21) Qin, Z.; Peng, R.; Baravik, I. K.; Liu, X. Fighting COVID-19: Integrated Micro- and Nanosystems for Viral Infection Diagnostics. *Matter* **2020**, *3*, 628−651.
(22) Wang, X.; Park, S.-G.; Ko, J.; Xiao, X.; Giannini, V.; Maier, S. A.; Kim, D.-H.; Choo, J. Sensitive and Reproducible Immunoassay of Multiple Mycotoxins Using Surface-Enhanced Raman Scattering Mapping on 3D Plasmonic Nanopillar Arrays. *Small* **2018**, *14*, No. 1801623.
(23) Li, M.; Cushing, S. K.; Zhang, J.; Suri, S.; Evans, R.; Petros, W. P.; Gibson, L. F.; Ma, D.; Liu, Y.; Wu, N. Three-Dimensional Hierarchical Plasmonic Nano-Architecture Enhanced Surface-Enhanced Raman Scattering Immunosensor for Cancer Biomarker Detection in Blood Plasma. *ACS Nano* **2013**, *7*, 4967−4976.
(24) Porter, M. D.; Lipert, R. J.; Siperko, N. M.; Wang, G.; Narayanan, R. SERS as a Bioassay Platform: Fundamentas, Design, and Applications. *Chem. Soc. Rev.* **2008**, *37*, 1001−1011.

https://doi.org/10.1021/acssensors.1c00596
ACS Sens. XXXX, XXX, XXX−XXX